Photonic Generation of Ultrawideband Signals

Jianping Yao, *Senior Member, IEEE, Member, OSA*, Fei Zeng, *Member, IEEE*, and Qing Wang

(Invited Paper)

***Abstract*—Ultrawideband (UWB) that is regulated by the Federal Communications Commission (FCC) for short-range high-throughput wireless communication and sensor networks with advantageous features, such as immunity to multipath fading, extremely short time duration, being carrier free, and having low duty cycle, wide bandwidth, and low power spectral density, has been a topic of interest recently. By wireless transmission, UWB communications systems can only operate in a short distance of a few meters to tens of meters. The convergence of UWB and optical fiber distribution techniques, or UWB over fiber, offers the availability of undisrupted service across different networks and eventually achieves high-data-rate access at any time and from any place. To distribute the UWB signals over the optical fiber, it is also desirable that the UWB signals can be generated in the optical domain without having extra electrical-to-optical conversion. In addition, UWB signals that are generated in the optical domain can be easily tailored to have a spectrum that meets the FCC-specified spectral mask. In this paper, techniques to generate UWB signals in the optical domain will be discussed. These techniques are divided into three categories, with the generation of UWB signals based on the following: 1) phase-modulation-to-intensity-modulation conversion, 2) a photonic microwave delay-line filter, and 3) optical spectral shaping and dispersion-induced frequency-to-time mapping. The areas for future development and the challenge of implementation of these techniques for practical applications will also be discussed.**

***Index Terms*—Dispersion, frequency-to-time mapping, microwave photonics, optical frequency discriminator, optical phase modulation, photonic microwave filter, radio over fiber, spectral shaping, ultrashort pulse, ultrawideband (UWB).**

I. Introduction

ULTRAWIDEBAND (UWB), which is regulated by the Federal Communications Commission (FCC) for indoor UWB systems operating in the frequency range from 3.1 to 10.6 GHz [1], has recently attracted considerable interests for short-range high-throughput wireless communications and sensor networks due to their intrinsic properties, such as immunity to multipath fading, extremely short time duration, being carrier free, and having low duty cycle, wide bandwidth, and low power spectral density [1]–[8]. Based on the FCC definition, a UWB signal should have a spectral bandwidth that is greater than 500 MHz or a fractional bandwidth that is greater than 20% [1]. There are, in general, two types of UWB: 1) the direct-sequence UWB [7] and 2) the multiband UWB [8]. Direct-sequence impulse radio is one of the most attractive techniques for UWB communications since it is carrier free; therefore, there is no need for complicated frequency mixers and local oscillators to down- or upconvert the carrier frequency. The selection of the impulse signal types is one of the fundamental considerations in designing an impulse UWB radio system, because the impulse types will determine the performance of the system [9]. For UWB communications, Gaussian pulses are the most widely used waveforms due to advantageous features, such as simplicity and achievability. Basically, a UWB waveform can be generated by passing a Gaussian pulse through a bandpass filter that acts in a manner that is similar to a first- or second-order frequency differentiator [2]. However, at the current stage of technology, it is rather difficult and expensive to generate such pulses with a fractional bandwidth that is greater than 100% at the central frequency of about 7 GHz [10]–[12].

On the other hand, by wireless transmission, UWB communications systems can only operate within a limited distance of a few meters to tens of meters. Such short-range wireless networks can operate mainly in an indoor environment in stand-alone mode, with a nearly nonexistent integration into fixed wired networks or wireless wide-area infrastructures. To offer availability of undisrupted service across different networks and to eventually achieve high-data-rate access at any time and from any place, UWB combined with fiber transmission, i.e., a technology called UWB over fiber, may provide an effective solution. Fig. 1 gives a conceptual illustration of a UWB-over-fiber system for broadband indoor wireless access. In the system, UWB pulses are generated and encoded in the central office (CO) and distributed to the access points (APs) via the optical fiber.

UWB pulses can be generated electrically using an electronic circuit, such as a microwave ring filter [10], a microwave resonator-based bandpass filter [11], or a microwave differentiator [12]. To distribute UWB signals over the optical fiber, it is highly desirable that the UWB signals can be generated directly in the optical domain without the need for extra electrical-to-optical conversion. In addition, the use of optical techniques

Manuscript received March 5, 2007; revised June 26, 2007. This work was supported by the Natural Sciences and Engineering Research Council of Canada (NSERC).

J. Yao and Q. Wang are with the Microwave Photonics Research Laboratory, School of Information Technology and Engineering, University of Ottawa, Ottawa, ON K1N 6N5, Canada (e-mail: jpyao@site.uOttawa.ca).

F. Zeng was with the Microwave Photonics Research Laboratory, School of Information Technology and Engineering, University of Ottawa, ON K1N 6N5, Canada. He is now with the Research Laboratory of Electronics, Massachusetts Institute of Technology, Cambridge, MA 02139 USA.

Color versions of one or more of the figures in this paper are available online at http://ieeexplore.ieee.org.

Digital Object Identifier 10.1109/JLT.2007.906820

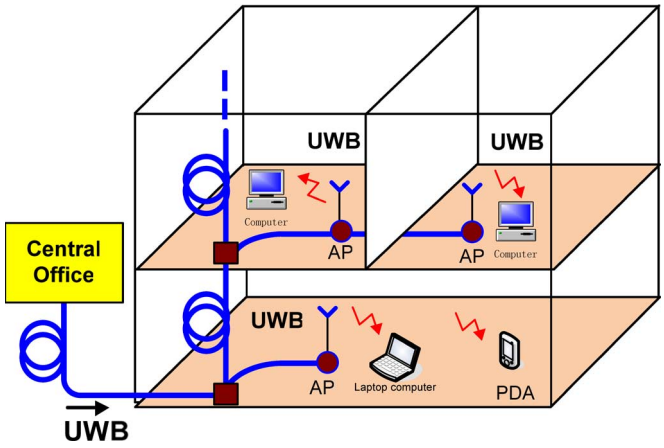

Fig. 1. UWB over fiber for broadband indoor wireless access (AP: access point).

to generate UWB pulses has many other advantages, such as light weight, small size, large tunability, and immunity to electromagnetic interference.

In this paper, techniques to generate UWB pulses in the optical domain will be discussed. These techniques can be classified into three categories: 1) UWB pulse generation based on phase-modulation-to-intensity-modulation (PM–IM) conversion (where the PM–IM conversion can be implemented in the optical domain by using either a dispersive device or an optical frequency discriminator) and 2) UWB pulse generation using a photonic microwave delay-line filter. To generate a UWB monocycle, a two-tap microwave delay-line filter with one negative coefficient is needed, while to generate a UWB doublet, a three-tap microwave delay-line filter with one negative coefficient is needed. The negative coefficient in the microwave delay-line filters can be generated based on cross-gain modulation (XGM) in a semiconductor optical amplifier (SOA) or cross-polarization modulation (XPolM) in a polarization modulator (PolM). 3) UWB pulse generation based on optical spectral shaping and dispersion-induced frequency-to-time mapping. The optical spectral shaping can be implemented using a spatial light modulator (SLM)-based or an optical-filter-based spectrum shaper to make the shaped spectrum have a shape corresponding to a UWB monocycle or doublet. The frequency-to-time mapping is realized using a dispersive device, such as a dispersive fiber. A comparison of these techniques is provided. The use of the techniques for UWB pulse coding is also briefly discussed.

II. UWB Pulse Generation Based on PM–IM Conversion

UWB pulse generation can be implemented in the optical domain based on optical PM–IM conversion. In this section, the principle of optical phase modulation will be discussed. Then, two different techniques to achieve PM–IM conversions, using either a dispersive device or an optical frequency discriminator, will be discussed. Optical implementations of these techniques will also be presented.

A. Optical Phase Modulation

The electrical field of a phase-modulated optical carrier $e_{\rm PM}(t)$ can be expressed as

$$e_{\rm PM}(t) = e_o \cos\left[\omega_o t + \Delta\varphi(t)\right] \tag{1}$$

where e_o and ω_o are the amplitude and the angular frequency of the optical carrier, and $\Delta\varphi(t)$ is the phase change that is induced by the modulating signal. Without loss of generality, $\Delta\varphi(t)$ can be expressed as

$$\Delta\varphi(t) = \beta_{\rm PM} \times f(t) \tag{2}$$

where $\beta_{\rm PM}$ is the phase modulation index, which is defined as the phase change of the optical carrier when a unit voltage is applied (radians per volt), and $f(t)$ is the electrical modulating signal.

If $f(t)$ is a single-frequency sinusoidal signal with zero initial phase, i.e.,

$$f(t) = V_e \cos\omega_m t \tag{3}$$

where V_e and ω_m are the amplitude and the angular frequency of the modulating signal, respectively, then (1) can be expanded in terms of Bessel functions of the first kind, i.e.,

$$e_{\rm PM}(t) = e_o \sum_{n=-\infty}^{+\infty} J_n(\beta_{\rm PM}V_e)\cos\left[(\omega_o + n\omega_m)t + \frac{1}{2}n\pi\right] \tag{4}$$

where $J_n(\cdot)$ denotes the nth-order Bessel function of the first kind. For simplicity, the argument $(\beta_{\rm PM}V_e)$ will be omitted in the remainder of this paper. From (4), we can see that the phase modulation generates a series of sidebands with amplitude coefficients that are determined by the Bessel functions. For small-signal modulation, only the first-order upper and lower sidebands need to be considered, and the higher order sidebands can be ignored.

With small-signal assumption, (4) can be further simplified as

$$e_{\rm PM}(t) = e_o\left\{J_o\cos\omega_o t + J_1\cos\left[(\omega_o+\omega_m)t + \frac{\pi}{2}\right] + J_{-1}\cos\left[(\omega_o-\omega_m)t - \frac{\pi}{2}\right]\right. . \tag{5}$$

For Bessel functions, we have

$$J_n = -J_{-n}, \qquad \text{when } n \text{ is odd.} \tag{6}$$

Applying the Fourier transform to the two sides of (5), we have

$$\begin{aligned} E_{\rm PM}(\omega) \approx{}& \pi e_o J_o\left[\delta(\omega-\omega_o)+\delta(\omega+\omega_o)\right] \\ &- j\pi e_o J_1\left[\delta(\omega+\omega_o+\omega_m)-\delta(\omega-\omega_o-\omega_m)\right] \\ &- j\pi e_o J_1\left[\delta(\omega+\omega_o-\omega_m)-\delta(\omega-\omega_o+\omega_m)\right]. \end{aligned} \tag{7}$$

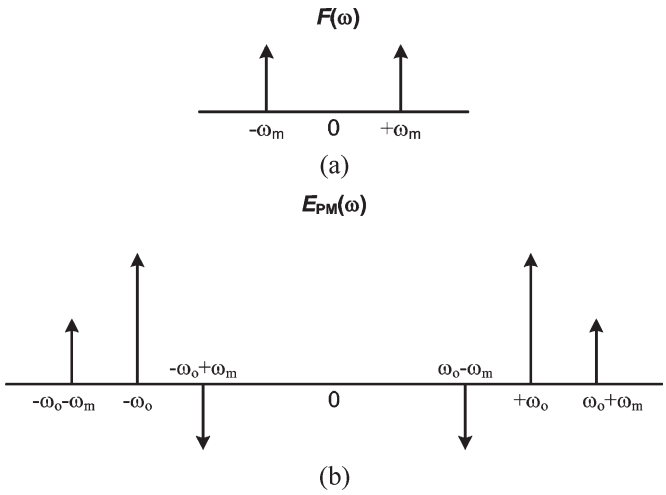

Fig. 2. Schematic showing the spectra of (a) single-frequency sinusoidal modulating signal and (b) phase-modulated optical signal.

Fig. 2 illustrates the spectra of the modulating electrical signal and the corresponding optical phase-modulated signal. From the figure, it is interesting to note that the lower sideband and upper sideband are exactly out of phase. If the phase-modulated signal is directly detected by a photodetector (PD), no signal, except a dc, will be generated since the beating between the lower sideband with the optical carrier will exactly cancel the beating between the upper sideband with the optical carrier.

B. PM–IM Conversion

To recover the information that is carried by the optical phase, a coherent detection based on a heterodyne or homodyne scheme can be used, in which the phase-modulated optical signal is mixed with a local oscillator light. However, it is difficult to build a local-oscillator light source with its phase that is locked to the input light source. In addition, the temperature and mechanical vibrations in the transmission line will result in phase and polarization fluctuations of the transmitted optical light, which would appear as noise after photodetection. Here, we will discuss two simple methods that were proposed recently to convert a phase-modulated signal to an intensity-modulated signal [13]–[15]. In the first method [13], [14], a dispersive device is used to change the phase relationship between the two first-order sidebands from out of phase to partially or fully in phase. In the second method [15], an optical filter is used to act as an optical frequency discriminator to perform PM–IM conversion. The operation of the latter method can be explained in that the magnitude relationships among the sidebands and the carrier are changed, leading to the PM–IM conversion. After the PM–IM conversion, a PD is then used to detect the intensity-modulated signal.

Fig. 3 shows the principle of the chromatic-dispersion-based PM–IM conversion, in which a phase-modulated signal propagates through a dispersive device and, then, is fed to a PD.

Assume that the dispersive device has a unity magnitude response (which is true if the dispersive device is a dispersive fiber with a very low loss) but a quadratic phase response. Then,

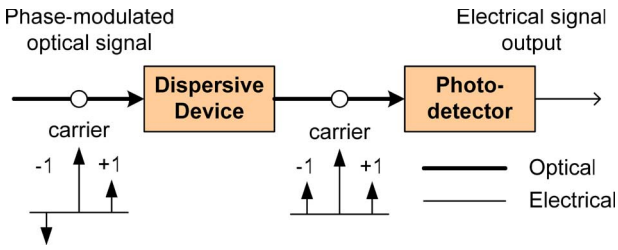

Fig. 3. Chromatic-dispersion-based PM–IM conversion and direct photodetection.

the optical signal at the output of the dispersive device can be expressed as

$$e_{\mathrm{DD}}(t) = e_o \cdot \Big\{ J_o \cos(\omega_o t + \theta_o) + J_1 \cos\Big[(\omega_o + \omega_m)t + \frac{\pi}{2} + \theta_{+1}\Big] - J_1 \cos\Big[(\omega_o - \omega_m)t - \frac{\pi}{2} + \theta_{-1}\Big] \quad (8)$$

where θ_o, θ_{-1}, and θ_{+1} are the phase shifts that are experienced by the optical carrier, the lower sideband, and the upper sideband, respectively.

Generally, a phase shift that is introduced by a dispersive device can be expressed as $\theta = \beta z$, where β is the propagation constant and z is the traveled distance. Expanding β in the Taylor series, we have

$$\theta = z\beta(\omega_o) + z\beta'(\omega_o)(\omega - \omega_o) + \frac{1}{2} \cdot z\beta''(\omega_o)(\omega - \omega_o)^2 + \cdots \quad (9)$$

where β' and β'' are the first- and second-order derivatives of β with respect to the optical angular frequency.

We know that group delay $\tau(\omega)$ is defined as $d\theta/d\omega$, i.e.,

$$\tau(\omega) \equiv \frac{d\theta}{d\omega} = z\beta'(\omega_o) + z\beta''(\omega_o)(\omega - \omega_o) + \cdots. \quad (10)$$

For a dispersive device with a quadratic phase response, its group delay response is linear. If the third- and higher order derivatives of β in (10) are ignored, (10) is simplified as

$$\tau(\omega) = \underbrace{z\beta'(\omega_0)}_{\tau_0} + z\beta''(\omega_0)(\omega - \omega_0) \quad (11)$$

where the first term (τ_0) is the group delay that is experienced by the optical carrier at frequency ω_0, and the second term describes the group delay variation as a linear function with respect to angular frequency ω.

The first-order chromatic dispersion is defined as the first-order derivative of the group delay with respect to angular frequency ω, which is a constant in this case, i.e.,

$$D_\omega = z\beta''(\omega_o). \quad (12)$$

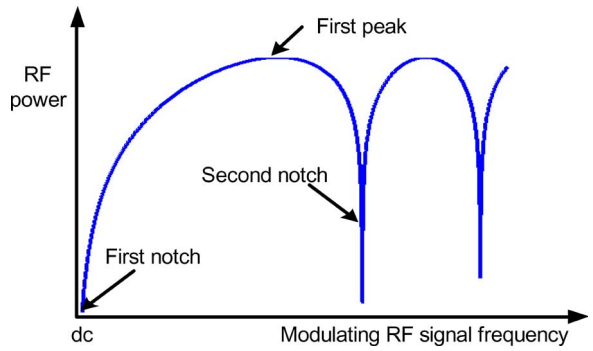

Fig. 4. Frequency response of the chromatic-dispersion-based PM–IM conversion.

Evaluating θ at the optical carrier of ω_0 and the sidebands of $\omega_o \pm \omega_m$, we have

$$\begin{cases} \theta_o = z\beta(\omega_o) \\ \theta_{-1} = z\beta(\omega_o) - \tau_o\omega_m + \frac{1}{2}D_\omega\omega_m^2 \\ \theta_{+1} = z\beta(\omega_o) + \tau_o\omega_m + \frac{1}{2}D_\omega\omega_m^2. \end{cases} \tag{13}$$

When the lightwave passes through a dispersive device, a photocurrent is generated at the PD. Taking only the RF signal that is centered at the modulating frequency ω_m and ignoring the dc current and the higher order harmonics, we have

$$\begin{aligned} i_{\mathrm{PD}} &\propto \sin\left(\frac{\theta_{+1}+\theta_{-1}}{2} - \theta_o\right) \cdot \cos\left(\omega_m t + \frac{\theta_{+1}-\theta_{-1}}{2}\right) \\ &= \underbrace{\sin\left(\frac{1}{2}D_\omega\omega_m^2\right)}_{H_{\mathrm{PM-IM}}(\omega_m)} \cdot \cos\left[\omega_m(t-\tau_o)\right]. \end{aligned} \tag{14}$$

From (14), we can see that the chromatic-dispersion-based PM–IM conversion with direct detection has a frequency response that is given by

$$H_{\mathrm{PM-IM}}(\omega_m) = \sin\left(\frac{1}{2}D_\omega\omega_m^2\right). \tag{15}$$

The frequency response is shown in Fig. 4, from which a quasi-periodic function with a notch at dc is observed. The first peak and the second notch can be determined by letting $D_\omega\omega_m^2/2 = \pi/2$ and π, respectively. The frequency response between the first two notches forms a passband, which can be directly used to shape the spectrum of the modulating signal. If the input modulating signal is a Gaussian pulse, the spectrum at lower frequency will be filtered out by the frequency response of the PM–IM conversion, a spectrum corresponding a Gaussian monocycle or doublet may be generated. In addition, the feature of PM–IM conversion with a notch at dc can be used to implement photonic microwave filters with bandpass functionality [13]–[18]. The baseband resonance of an optical microwave filter with all-positive coefficient can be eliminated by the dc notch of the frequency response of the chromatic-dispersion-based PM–IM conversion.

Optical PM–IM conversion can also be implemented using an optical frequency discriminator. Based on the theoretical analysis in Section II-A, a phase-modulated signal has two sidebands that are out of phase. If the phase relationship between the two sidebands can be changed to partially or totally in phase, PM–IM conversion is realized. This is the basis of chromatic-dispersion-based PM–IM conversion. On the other hand, if the magnitude relationship among the optical carrier and the sidebands is changed, the PM–IM conversion can also be realized. For instance, using an optical filter to eliminating either one sideband or the carrier would lead to the PM–IM conversion. In the following, a general discussion on optical-filter-based PM–IM conversion is presented, in which an optical bandpass filter having two linear slopes is used as a frequency discriminator.

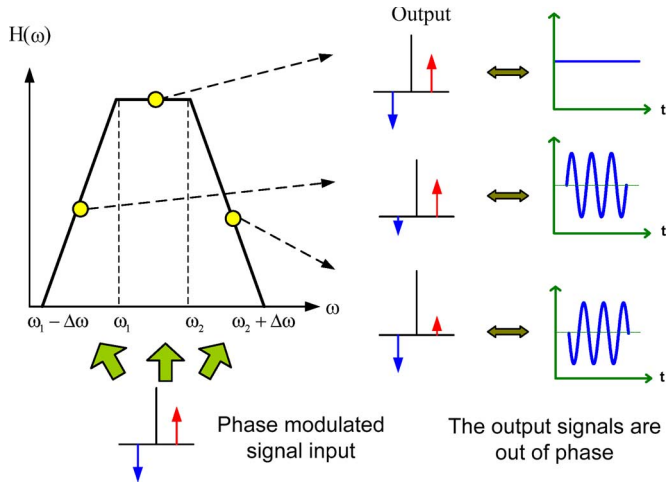

Fig. 5. Ideal frequency response of an optical filter with two linear slopes and a flat top.

Fig. 5 shows the frequency response of an ideal optical filter. It has two linear slopes; by locating the carrier of the phase-modulated signal at one of the two slopes, PM–IM conversion is realized.

Mathematically, the frequency response of the optical filter that is shown in Fig. 5 can be written as

$$|H_d(j\omega)| = \begin{cases} K\omega - K(\omega_1 - \Delta\omega) & \\ \quad \omega_1 - \Delta\omega \le \omega \le \omega_1, & \text{left slope} \\ K \cdot \Delta\omega, \quad \omega_1 \le \omega \le \omega_2, & \text{center} \\ K(\omega_2 + \Delta\omega) - K\omega & \\ \quad \omega_2 \le \omega \le \omega_2 + \Delta\omega, & \text{right slope} \\ 0, & \text{otherwise} \end{cases} \tag{16}$$

where K is the slope of the filter $(K > 0)$, and ω is the optical frequency. From (16), we can see that the frequency response of the optical filter consists of three linear sections: 1) the left slope; 2) the center; and 3) the right slope. To simplify the analysis, we assume that, within each section, the phase response is linear. This assumption was verified to be acceptable if the filter is a fiber Bragg grating (FBG) with proper apodization. In addition, if the phase-modulated optical signal has a narrow bandwidth and the optical carrier is properly selected to make it located at the center of each spectral section of the frequency response of the optical filter, as shown in

Fig. 5, the impulse response of the optical filter $h_d(t)$ can be approximated as

$$h_d(t) \approx \begin{cases} -K(\omega_1 - \Delta\omega)\delta(t) - jK\delta'(t), & \text{left slope} \\ K\Delta\omega\delta(t), & \text{center} \\ K(\omega_2 + \Delta\omega)\delta(t) + jK\delta'(t), & \text{right slope} \end{cases} \tag{17}$$

where the group delay that was derived from the linear phase response is neglected, $\delta(t)$ is the unit impulse, and $\delta'(t)$ is the first-order derivative of the unit impulse. Note that $\delta(t) \overset{FT}{\longleftrightarrow} 1$ and that $(d/dt)x(t) \overset{FT}{\longleftrightarrow} j\omega \cdot X(\omega)$. After the phase-modulated optical signal passing through the optical filter, we obtain the optical field

$$\begin{aligned} e_d(t) &= e_{\mathrm{PM}}(t) * h_d(t) \\ &\approx \begin{cases} e_{\mathrm{PM}}(t)\left[K(\omega_o - \omega_1 + \Delta\omega) + K\beta_{\mathrm{PM}}f'(t)\right], & \text{left slope} \\ e_{\mathrm{PM}}(t)K\Delta\omega, & \text{center} \\ e_{\mathrm{PM}}(t)\left[K(\omega_2 + \Delta\omega - \omega_o) - K\beta_{\mathrm{PM}}f'(t)\right], & \text{right slope} \end{cases} \end{aligned} \tag{18}$$

where $*$ denotes the convolution operation, and $f'(t)$ is the first-order derivative of the modulating signal $f(t)$. Again, the photocurrent at the output of the PD is given by

$$i_{PD}(t) \sim \begin{cases} PK^2\left\{(\omega_o - \omega_1 + \Delta\omega)^2 + [\beta_{PM}f'(t)]^2 + 2(\omega_o - \omega_1 + \Delta\omega)\beta_{PM}f'(t)\right\}, & \text{left slope} \\ PK^2\Delta\omega^2, & \text{center} \\ PK^2\left\{(\omega_2 + \Delta\omega - \omega_o)^2 + [\beta_{PM}f'(t)]^2 - 2(\omega_2 + \Delta\omega - \omega_o)\beta_{PM}f'(t)\right\}, & \text{right slope} \end{cases} \tag{19}$$

where P is the optical power at the input of the PD. The first term on the right-hand side for each case, which is equal to $|H_d(\omega)|_{\omega=\omega_o}$, represents a dc component and can be eliminated by using a dc blocker. When optical carrier ω_0 is located at the left or right slope with an assumption of small-signal modulation, the second term is much smaller than the third term and can be neglected. Finally, we obtain the recovered RF signal

$$r(t) \sim \begin{cases} 2PK^2(\omega_o - \omega_1 + \Delta\omega)\beta_{\mathrm{PM}}f'(t), & \text{left slope} \\ 0, & \text{center} \\ -2PK^2(\omega_2 + \Delta\omega - \omega_o)\beta_{\mathrm{PM}}f'(t), & \text{right slope.} \end{cases} \tag{20}$$

From (20), we can conclude the following: 1) No signal can be recovered if the optical carrier is located at the center passband of the optical filter. 2) The recovered signal is proportional to the first-order derivative of the modulating signal when the optical carrier is located at either slope of the optical filter. 3) The detected signals have different signs when the carriers are located at the opposite slopes, which is a very important feature and would find many interesting applications in all-optical microwave signal processing [19], [20].

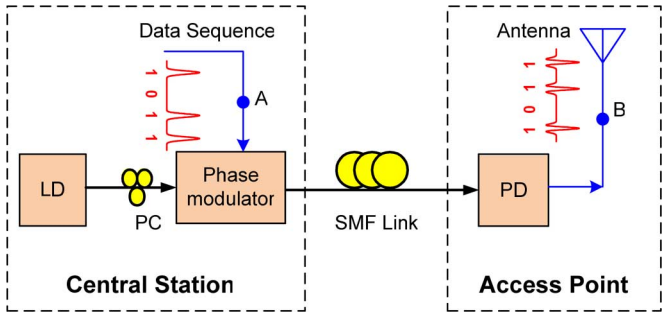

Fig. 6. UWB generation system based on PM–IM conversion in a dispersive device. The dispersion device is a length of SMF (LD: laser diode, PD: photodetector, PC: polarization controller).

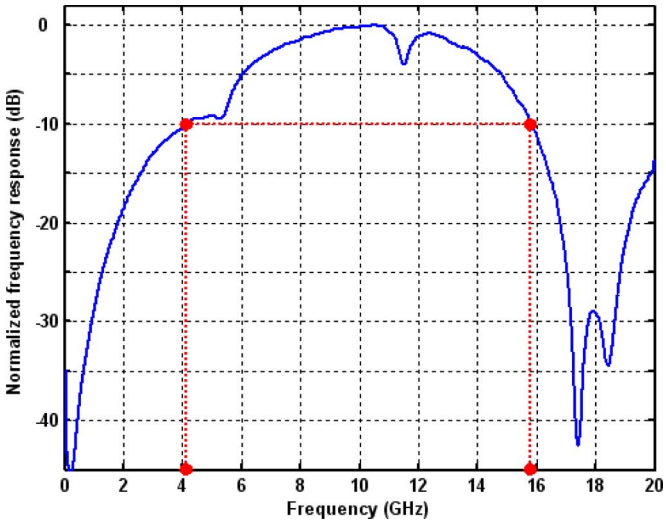

Fig. 7. Frequency response of the UWB pulse generation system based on PM–IM conversion in a dispersive device.

C. UWB Pulse Generation Based on PM–IM Conversion in a Dispersive Device

As discussed in Section II-B, PM–IM conversion in a dispersive device has a frequency response corresponding to a bandpass filter. If the filter is properly designed by taking into consideration the frequency responses of the phase modulator and the PD, then the spectrum of a Gaussian pulse can be shaped to have a spectrum that satisfies the FCC spectrum mask. Fig. 6 shows a system to generate and distribute UWB signals over a standard single-mode fiber (SMF) [21]. As can be seen, an AP is connected to a central station (CS). At the CS, a lightwave from a laser diode (LD) is fed to an optical phase modulator, which is driven by a data sequence to be transmitted. The phase-modulated optical signal is then transmitted to the AP via a length of SMF, which serves as a transmission medium as well as a dispersive device. Due to the chromatic dispersion that is induced by the SMF, at the AP, the phase-modulated signal is converted to an intensity-modulated signal, and the electrical signal is obtained at the output of a PD, which is ready to radiate to the space via an UWB antenna.

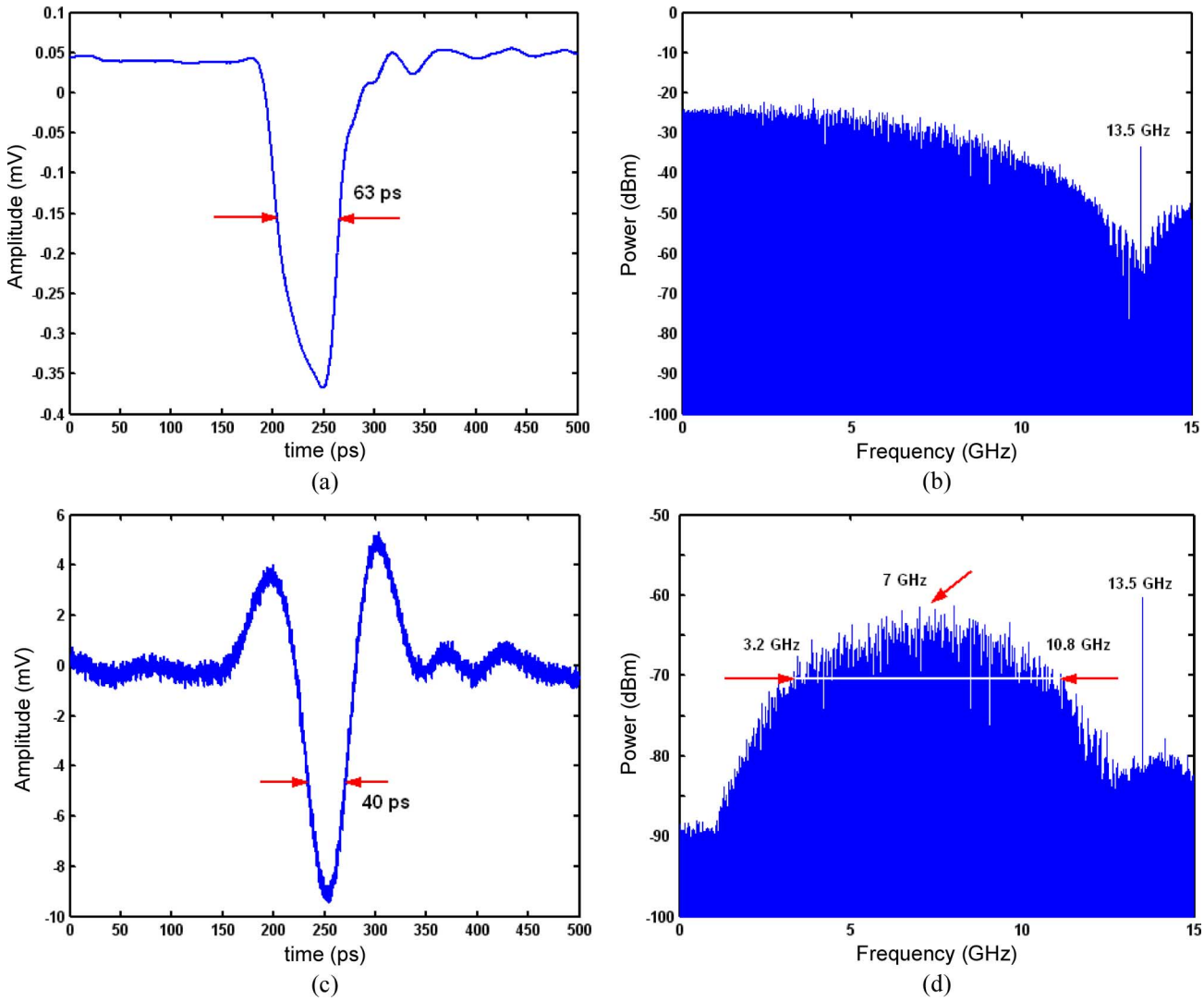

Fig. 8. (a) Waveform of a Gaussian-like input pulse. (b) Power spectrum of the Gaussian-like pulse. (c) Generated UWB doublet. (d) Power spectrum of the doublet.

Under small-signal condition, the frequency response of the system, including the frequency responses of the phase modulator and the PD, is given by

$$H(\omega) = \sin\left(\frac{1}{2}D_\omega \omega_m^2\right) \times H_{\mathrm{PM}}(\omega) \times H_{\mathrm{PD}}(\omega) \qquad (21)$$

where the first term on the right-hand side is the frequency response of the PM–IM conversion, which is given in (15), and $H_{\mathrm{PM}}(\omega)$ and $H_{\mathrm{PD}}(\omega)$ are the frequency responses of the phase modulator and the PD, respectively. Since the frequency responses of the phase modulator and the PD are usually bandwidth limited, the overall frequency response of the system can be limited to a passband that is close to dc. In addition, since the frequency response of the PM–IM conversion depends on the optical carrier wavelength and the total dispersion of the transmission medium, the bandwidth and shape of the bandpass filter can be tailored by changing the carrier wavelength and the total dispersion to optimize the spectrum of the generated UWB signals. Fig. 7 shows an experimental frequency response of the system, with the LD operating at 1550 nm and an SMF length of 25 km. The SMF has a chromatic dispersion of 17 ps/nm · km at 1550 nm, with 25 km of this fiber having a total dispersion of 425 ps/nm. From Fig. 7, we can see that a notch at the dc is observed. The passband peak and the lower and higher −10-dB cutoff frequencies are 10.5, 4.1, and 15.9 GHz, respectively.

Then, a Gaussian-like pulse with a full-width at half-maximum (FWHM) of about 63 ps is applied to the phase modulator via its RF port. The temporal shape and the spectrum of the input pulse are shown in Fig. 8(a) and (b). After passing through the 25-km SMF link, the phase-modulated optical signal is converted to an intensity-modulated signal, which is then detected by the PD at the AP. Fig. 8(c) shows the temporal waveform of the generated pulse, which is a Gaussian doublet with an FWHM of about 40 ps. The spectrum of the doublet is shown in Fig. 8(d). It can be seen that the spectrum has a central frequency of about 7 GHz, and the lower and higher frequencies at −10 dB points are 3.2 and 10.8 GHz, respectively. The generated UWB doublet has a fractional bandwidth of about 109%.

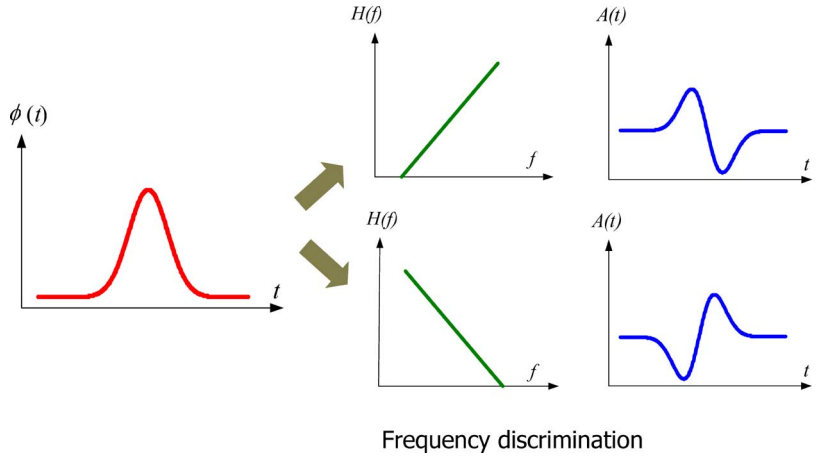

Fig. 9. UWB monocycle generation using a linear optical frequency discriminator.

D. UWB Pulse Generation Based on PM–IM Conversion in an Optical Frequency Discriminator

The technique to generate UWB pulses that was discussed in Section II-C requires the use of a dispersive element, which was the 25-km SMF in the experiment. There are two limitations that are associated with the use of optical fiber as a dispersive device. First, the fiber length is long. For most of the applications, the communication distance is much less than 25 km; therefore, the system is bulky. Second, the fiber should have a fixed length to achieve a desirable frequency response. If the communication distance is changed with a different fiber length, the frequency response of the system is changed, leading to a distortion in the generated UWB pulses. A method to avoid using a long optical fiber is to use an optical-filter-based frequency discriminator to perform PM–IM conversion [22]. The theoretical details of an optical frequency discriminator have been discussed in Section II-B. If a phase-modulated Gaussian pulse is sent to an optical frequency discriminator, depending on the location of the optical carrier at the linear or quadrature slope, a Gaussian monocycle or doublet would be generated. In addition, the location of the optical carrier at the positive or negative slope would lead to the generation of UWB pulses with opposite polarity. Fig. 9 shows the generation of a UWB monocycle using a linear optical frequency discriminator.

For real implementation, the optical frequency discriminator can be an optical filter, such as an FBG [22]. Fig. 10 shows the reflection spectrum of a 10-mm apodized FBG with a central wavelength of 1536.12 nm, a 3-dB bandwidth of 0.23 nm, and a reflectivity of 90%. By locating the optical carrier with phase modulation of a Gaussian pulse at the linear slope or the quadrature of the FBG reflection spectrum, a UWB monocycle or doublet pulse is obtained at the output of a PD. In addition, UWB pulses with opposite polarities can be generated by locating the optical carrier at the right or left slope of the FBG reflection spectrum. This property provides the possibility of implementing two different UWB pulse modulation schemes by simply shifting the optical carrier: 1) the pulse shape modulation (PSM) (monocycle-doublet) and 2) the pulse polarity modulation (PPM).

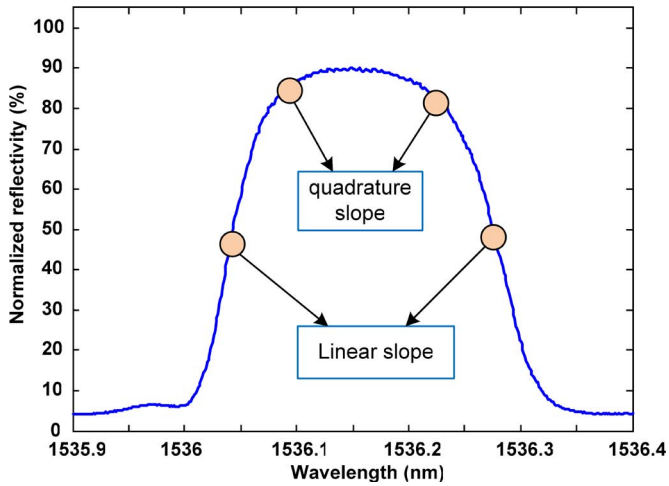

Fig. 10. Reflection spectrum of an apodized FBG.

Fig. 11 shows an experimental setup to generate UWB pulses based on PM–IM conversion in an optical frequency discriminator. The lightwave from an LD is fed to an optical phase modulator that is driven by an electrical Gaussian pulse. The phase-modulated optical signal is then applied to an FBG via an optical circulator. The PM–IM conversion is achieved by using the FBG serving as a frequency discriminator. The PM–IM converted signal is then detected at a PD.

Based on the configuration that is shown in Fig. 11, when the phase-modulated light is located at the linear region of the FBG reflection slopes, as shown in point A in Fig. 11, the AC part of the recovered signal at the output of the PD can be written as

$$r(t) \sim \Re P \beta_{\mathrm{PM}} K^2 s'(t) \tag{22}$$

where $\Re$ is the responsivity of the PD, P is the optical power reflected from the FBG, K is the slope of the FBG power spectrum, and $s'(t)$ is the first-order derivative of the modulating signal $s(t)$. A UWB monocycle is thus generated.

When the optical carrier is located at the opposite slope of the FBG reflection spectrum, as shown in point D in Fig. 11, the output pulse will be a monocycle with an opposite polarity. This feature enables the realization of PPM when two optical

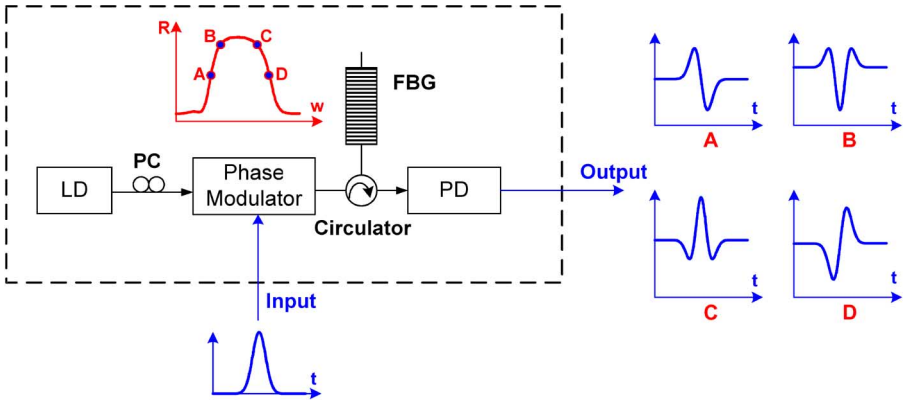

Fig. 11. Experimental setup for UWB pulse generator based on PM–IM conversion in an optical frequency discriminator.

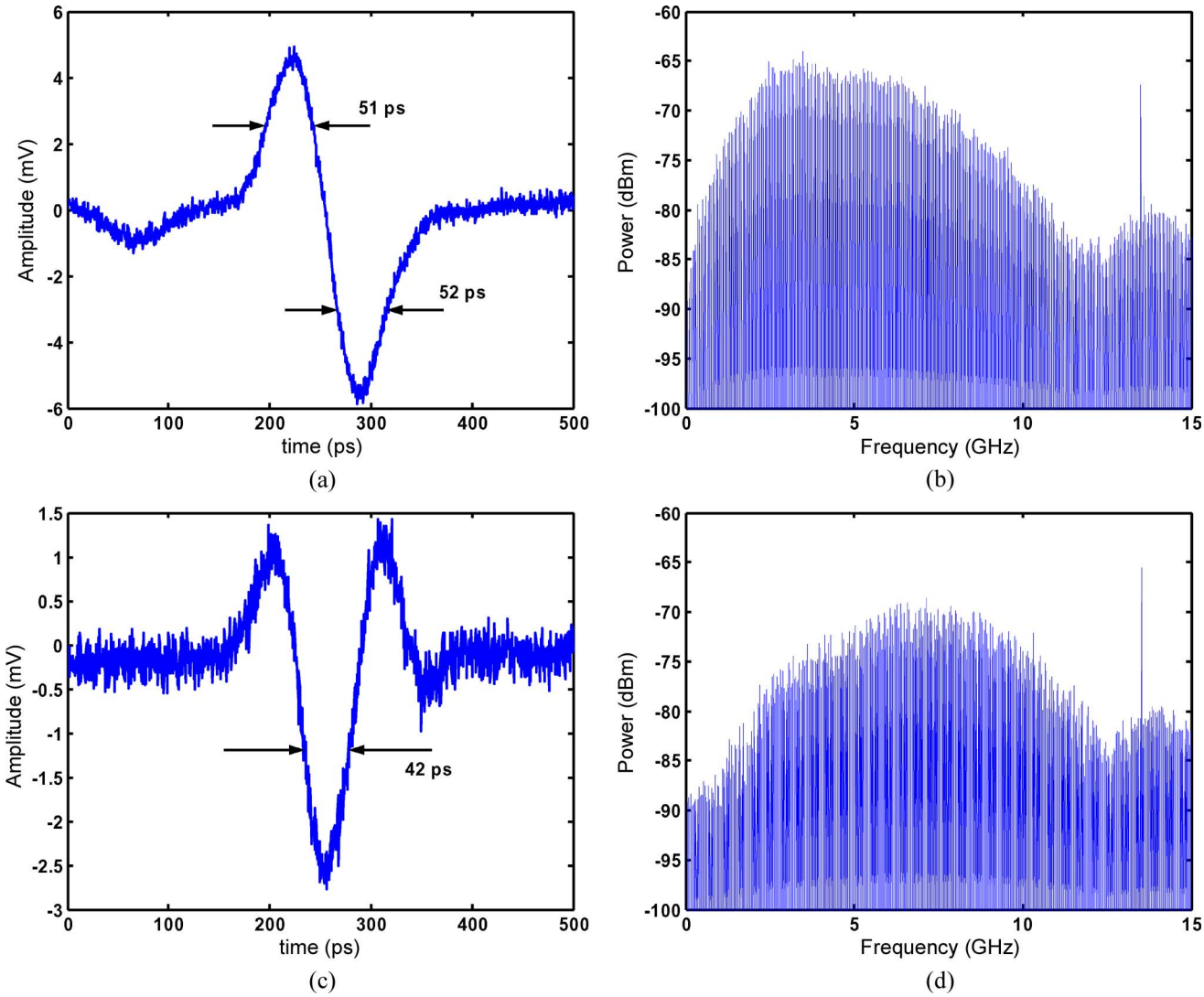

Fig. 12. (a) Waveform of the generated Gaussian monocycle and (b) the corresponding power spectrum. (c) Waveform of the generated Gaussian doublet and (d) the corresponding power spectrum.

carriers corresponding to these two complementary pulses are employed and switched by a data sequence to be transmitted. In addition, if the optical carrier is located at the quadrature slopes of the FBG reflection spectrum, as shown in points B and C in Fig. 11, UWB doublets are generated. Therefore, by locating the optical carrier at different locations, UWB pulses with different shapes can be generated in the same configuration, and eventually, the implementation of PSM is possible.

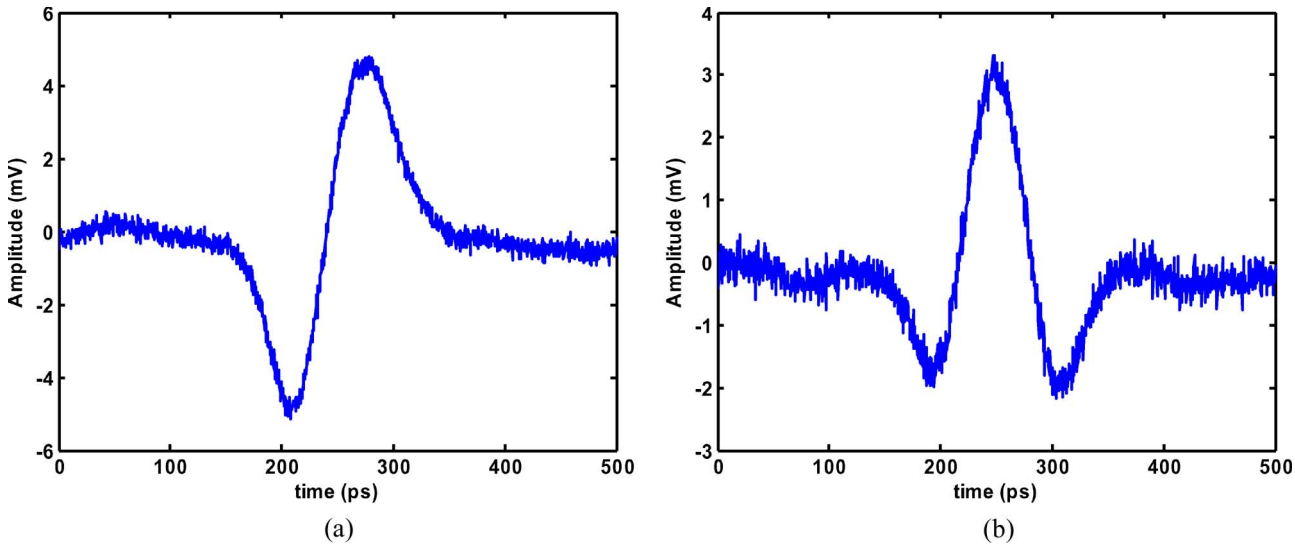

Fig. 13. Waveforms of the Gaussian monocycle and doublet when the optical carrier is located at the opposite slopes of the FBG.

Experimental results are shown in Fig. 12. When the carrier wavelength is tuned to 1536.032 nm, which is located at the left linear slope of the FBG spectrum that is shown in Fig. 10, a Gaussian monocycle pulse is generated, as shown in Fig. 13(a). The spectrum of the generated Gaussian monocycle is shown in Fig. 12(b), which has a central frequency of about 3.45 GHz, and a 10-dB bandwidth of about 7.94 GHz. When the carrier wavelength is tuned at 1536.098 nm, which is located at the left turning corner (quadrature slope) of the FBG spectrum, the generated pulse is a Gaussian doublet, as shown in Fig. 12(c). From its power spectrum shown in Fig. 12(d), we can see that the central frequency is increased to 7.14 GHz, and the 10-dB bandwidth is about 8.8 GHz. These results are expected according to the mathematical definition of a Gaussian pulse with different orders of derivatives [23].

When the wavelength of the optical carrier is tuned to be reflected at the right turning corner and the right linear slopes of the FBG spectrum, the generated pulses, which are shown in Fig. 13, are the inverted versions of those shown in Fig. 12(a) and (c).

We should note that, in the systems that are shown in Figs. 6 and 11, the input Gaussian pulse is generated electrically using a pulse generator, and the phase modulation is implemented using an optical phase modulator. Therefore, the two systems are not all optical but hybrid. To generate UWB pulses using an all-optical system, the Gaussian pulse should be generated in the optical domain. One possible solution is to generate the Gaussian pulse using a mode-locked pulse laser source. In addition, the optical phase modulation should also be implemented in the optical domain, which can be realized based on optical cross-phase modulation (XPM). Optical XPM can be implemented in an optical nonlinear device, such as the length of the nonlinear fiber.

Fig. 14 shows an all-optical UWB pulse generation system [24]. It is different from the system that is shown in Fig. 11, where the Gaussian pulse is generated using an electrical pulse generator; in the system that is shown in Fig. 14, the optical Gaussian pulse is generated using a femtosecond pulse laser

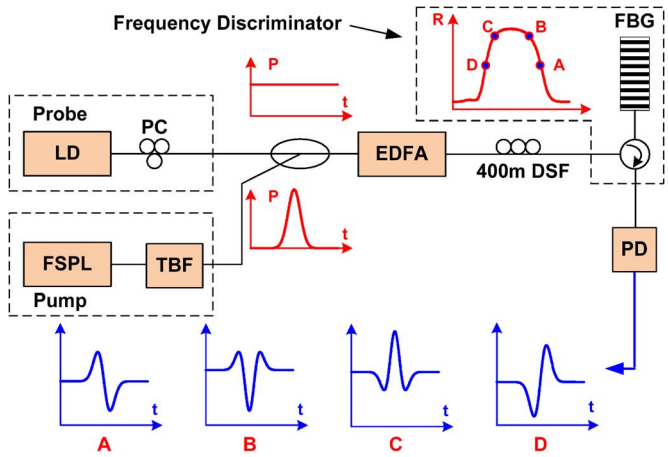

Fig. 14. All-optical UWB pulse generator. The Gaussian pulse is generated by the FSPL with proper spectrum slicing to control the pulsewidth. XPM is realized in the 400-m DSF.

(FSPL), and the phase modulation is implemented based on XPM in a length of nonlinear fiber. To control the pulsewidth, a tunable bandpass filter is incorporated after the FSPL. The generated optical pulse is then injected with a continuous-wave (CW) probe into a length of dispersion-shifted fiber (DSF) to achieve optical XPM. The phase-modulated signal that is carried by the probe is then converted to an intensity-modulated signal at an FBG (serving as a frequency discriminator). The FBG also serves as an optical bandpass filter to remove the residual pump and the amplified spontaneous emission (ASE) noise from the erbium-doped fiber amplifier (EDFA). Depending on the location of the probe at the FBG reflection spectrum, a UWB monocycle or doublet is generated.

III. UWB Pulse Generation Based on a Photonic Microwave Delay-Line Filter

It is known that a Gaussian monocycle or doublet is the first- or second-order derivative of a Gaussian pulse [23].

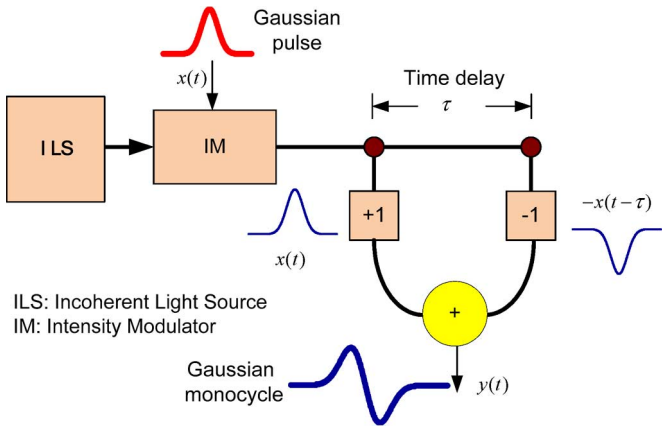

Fig. 15. UWB monocycle generation based on a two-tap microwave delay-line filter with one negative coefficient.

The first- or second-order derivative can be implemented in the optical domain using an optical frequency discriminator [22], as discussed in Section II-B, and its experimental demonstration, as discussed in Section II-D. The approach that was discussed in Section II-B, which uses a dispersive device to perform PM–IM conversion, can also be considered as a frequency discriminator [21]. Mathematically, the first- and the second-order derivatives can be approximated by the first- and second-order differences, which can be implemented using a photonic microwave delay-line filter, with two or three taps, both with one negative tap. It is known that, to design a photonic microwave delay-line filter, to avoid optical interference, the filter should operate in the incoherent regime using incoherent detection. A photonic microwave delay-line filter with incoherent detection can usually have positive coefficients only [25]–[27]. Therefore, to generate a negative coefficient while maintaining incoherent detection, special designs must be incorporated. In this section, two methods to generate a negative coefficient will be discussed. In the first method, a negative coefficient is generated based on XGM in an SOA by injecting two wavelengths, with one saving as the pump and the other as the probe. In the second method, a PolM is used. The negative coefficient is generated based on polarization modulation in a PolM.

A. Photonic Microwave Delay-Line Filters for UWB Pulse Generation

Assume that $x(t)$ is the input Gaussian pulse that is applied to a two-tap microwave delay-line filter with one positive and one negative coefficient of [1 −1], as shown in Fig. 15. The output $y(t)$ is given by

$$y(t) = x(t) - x(t-\tau) \tag{23}$$

where τ is the time-delay difference. Applying Fourier transform to the two sides of (23), we have

$$Y(\omega) = X(\omega) - e^{-j\omega\tau}X(\omega) = X(\omega)(1 - e^{-j\omega\tau}) \tag{24}$$

where $Y(\omega)$ and $X(\omega)$ are the Fourier transforms of $y(t)$ and $x(t)$, respectively. The magnitude frequency response of the filter is given by

$$|H(\omega)| = \left|\frac{Y(\omega)}{X(\omega)}\right| = \sqrt{2 - 2\cos(\omega\tau)}. \tag{25}$$

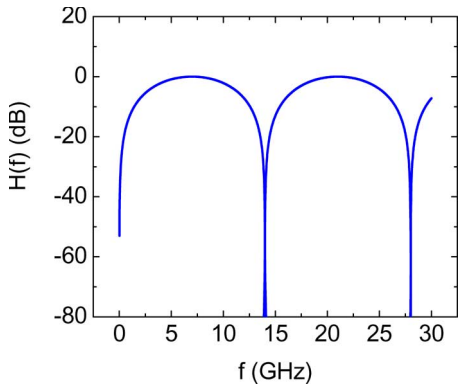

Fig. 16. Magnitude frequency response of a two-tap microwave delay-line filter with coefficients [1 −1] and a time-delay difference of $\tau = 70$ ps.

Fig. 16 shows the frequency response of the two-tap microwave delay-line filter with a time-delay difference of $\tau = 70$ ps. As can be seen, the filter is a bandpass filter with the center frequency of the first passband located at 7 GHz. For practical applications, considering the limited bandwidth of the intensity modulator and the PD, the resonances at higher frequencies can be ignored. Therefore, by properly selecting time-delay difference τ, a filter with a frequency response that can shape the spectrum of the input Gaussian pulse to have a spectrum corresponding to a UWB monocycle would be obtained.

A UWB doublet can be generated by implementing the second-order derivative of a Gaussian pulse, which can be approximated by the second-order difference

$$\begin{aligned} y(t) &= [x(t) - x(t-\tau)] - [x(t-\tau) - x(t-2\tau)] \\ &= x(t) - 2x(t-\tau) + x(t-2\tau). \end{aligned} \tag{26}$$

From (26), we can see that a UWB doublet can be generated using a microwave delay-line filter with three taps with coefficients of [1 −2 1], as shown in Fig. 17. The frequency response of the three-tap microwave delay-line filter is given by

$$H(\omega) = \frac{Y(\omega)}{X(\omega)} = 1 - 2e^{-j\omega\tau} + e^{-2j\omega\tau}. \tag{27}$$

The magnitude frequency response is shown in Fig. 18. It is a bandpass filter with a narrower frequency response compared to that of the two-tap microwave delay-line filter that is shown in Fig. 16. Because of the narrower frequency response, the Gaussian pulse is shaped to have a spectrum corresponding to a Gaussian doublet.

B. UWB Monocycle Generation With a Two-Tap Microwave Delay-Line Filter

In this section, two demonstrations of two-tap microwave delay-line filters with coefficients of [1 −1] for Gaussian monocycle generation will be discussed. In the first filter, the

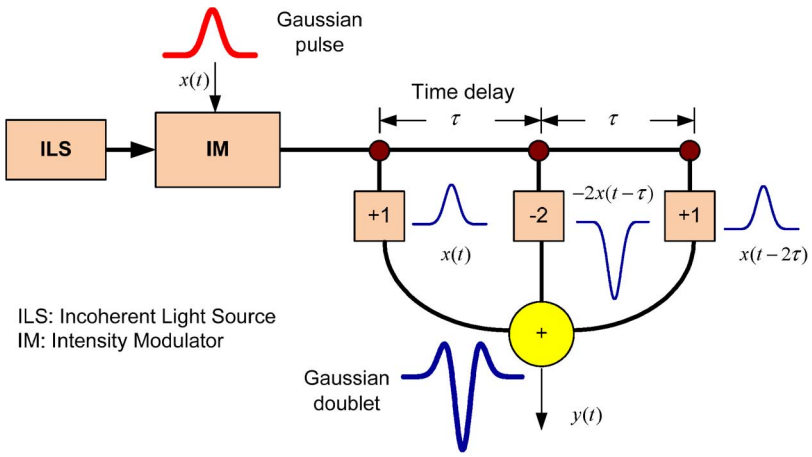

Fig. 17. UWB doublet generation based on a three-tap delay-line filter with coefficients [1 −2 1] and a time-delay difference of $\tau = 70$ ps.

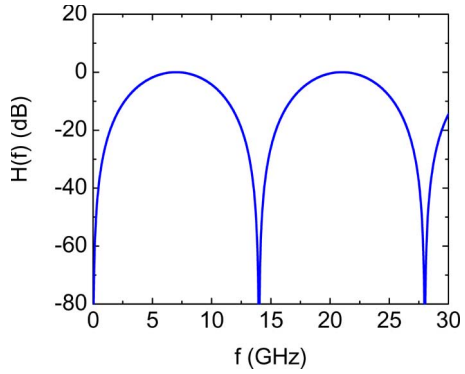

Fig. 18. Magnitude frequency response of a three-tap microwave delay-line filter with coefficients [1 −2 1] and a time-delay difference of $\tau = 70$ ps.

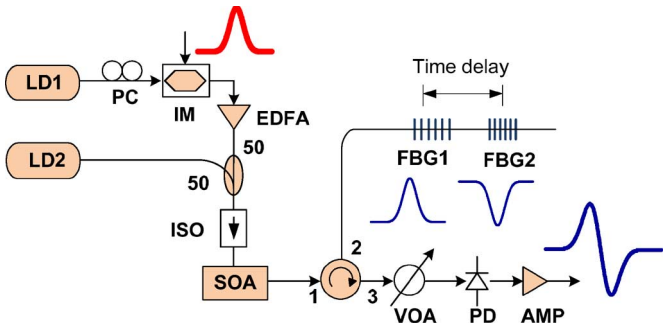

Fig. 19. UWB monocycle generation based on a two-tap photonic microwave delay-line filter using an SOA (PC: polarization controller, IM: intensity modulator, EDFA: erbium-doped fiber amplifier, ISO: isolator, SOA: semiconductor optical amplifier, VOA: variable optical attenuator, AMP: amplifier).

negative coefficient is generated based on XGM in an SOA. In the second filter, a PolM is used to generate the negative coefficient.

Fig. 19 shows a two-tap microwave delay-line filter with one negative coefficient implemented using an SOA for UWB monocycle generation [28]. The function of the SOA in the system is to generate a negative coefficient based on XGM. As shown in Fig. 19, two lightwaves, in which one is a high-power pulsed lightwave (the pump, which is modulated by a Gaussian pulse) and the other is a low-power CW lightwave (the probe), are both injected into the SOA. Due to the XGM, the power of the probe would vary inversely with the pump power; a pair of complementary optical pulses are thus generated, with one at the pump wavelength and the other at the probe wavelength. If a proper time-delay difference is introduced between the two pulses, a monocycle is generated. The pulsewidth of the monocycle can be controlled by altering the time-delay difference to make its spectrum meet the FCC spectrum mask.

Fig. 20 shows the generated monocycle and its spectrum. In the experiment, a Gaussian pulse with an FWHM of about 72 ps is applied to the intensity modulator. The output from the intensity modulator, which is amplified by an EDFA, is injected into the SOA with a probe that is generated by a second LD. Due to the XGM, a pair of polarity-reversed pulses are generated at the output of the SOA. The time-delay difference between the two pulses is introduced by two FBGs. The two FBGs are fabricated in a hydrogen-loaded SMF with a physical spacing of $L = 5$ mm between the two FBGs. Since the pump power is higher than the probe power, the amplitudes of the two pulses are different. To have a good Gaussian monocycle, FBG1 is made with a much lower reflectivity than FBG2. In addition to the introduction of the time-delay difference, the two FBGs also function as two optical bandpass filters to filter out the ASE noise that is generated by the SOA. The FWHM of the monocycle pulse is about 48 ps, which is narrower than that of the original Gaussian pulse. This is because the time-delay difference between the pump and a probe pulse is smaller than the width of the Gaussian pulse. The envelope of the discrete spectrum lines corresponds to the spectrum of a single monocycle pulse, which has a center frequency at about 5.0 GHz and a −10-dB bandwidth of about 9.4 GHz, with a fractional bandwidth of about 188%. It is different from the UWB generation schemes that were discussed in Sections II-C and D, where a single wavelength is used; the system here employs two wavelengths. When the UWB pulse is distributed over fiber, the fiber chromatic dispersion effect would have a higher impact compared with the approaches using a single wavelength, as the wavelength spacing between the two wavelengths is usually larger than the spectrum bandwidth of the UWB pulse.

Note that the two FBGs in the system can be replaced by a dispersive device, such as a dispersive fiber or a chirped

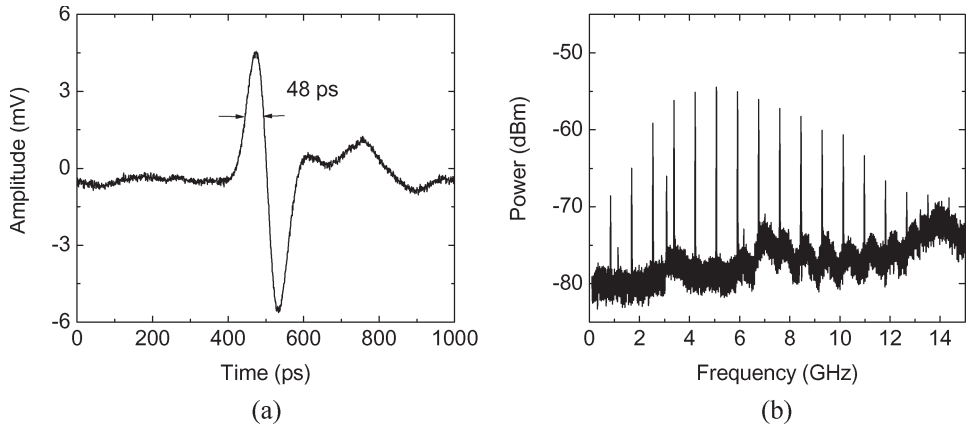

Fig. 20. Generated UWB monocycle pulse. (a) Temporal waveform and (b) its spectrum.

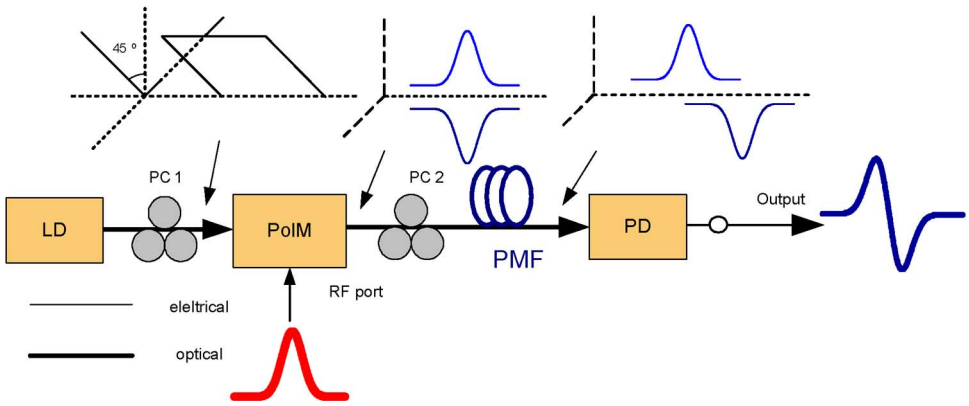

Fig. 21. UWB monocycle generation using a two-tap microwave delay-line filter based on a PolM.

FBG. Due to the chromatic dispersion, the two pulses will travel in the dispersive device at different velocities; a time-delay difference would be generated. The advantage of using a dispersive device is that the time-delay difference can be easily tuned by tuning the wavelength spacing between the pump and the probe wavelengths.

To avoid using two wavelengths, we may use a different architecture in which the negative coefficient is generated using a PolM. We have recently demonstrated a two-tap photonic microwave bandpass filter with one negative coefficient using a PolM [29]. The same architecture can be employed for UWB monocycle generation if the input modulating signal is a Gaussian pulse. Fig. 21 shows a PolM-based UWB monocycle generation system. As can be seen, a single wavelength that is generated by an LD is sent to the PolM via a polarization controller (PC) to align it polarization direction with an angle of 45° to one principal axis of the PolM. A Gaussian pulse is applied to the PolM via its RF port. Due to the polarization modulation, two complementary Gaussian pulses that are modulated on two orthogonally polarized optical carriers are generated. The optical signals are then sent to a polarization-maintaining fiber (PMF)-based delay line through a second PC (PC2) to align its polarization directions with the principal axes of the PMF to introduce a time-delay difference. The time-delay difference is determined by the birefringence of the PMF and the length the PMF. The time-delayed Gaussian pulses are then detected at a PD.

C. UWB Doublet Generation With a Three-Tap Microwave Delay-Line Filter

The two-tap microwave delay-line filter that is shown in Figs. 19 and 21 can generate a UWB monocycle using an SOA or a PolM. The filter architectures can be modified to generate a Gaussian doublet. As discussed in Section III-A, to generate a UWB doublet, a three-tap microwave delay-line filter with coefficients of [1 −2 1] is needed. Figs. 22 and 23 show two architectures: One is based on an SOA, and the other is based on a PolM, for Gaussian doublet generation.

The difference between the filters in Figs. 19 and 22 is that, in Fig. 22, two CW probes are used. Again, due to the XGM in the SOA, the pulses that are carried by the two probes are both inverted versions of the one that is carried by the pump. If the three pulses are reflected by three FBGs with a proper time-delay difference and a reflectivity ratio of 1 : 2 : 1, a UWB doublet is generated.

In Fig. 23, three wavelengths that are generated by three LDs are sent to the PolM. The polarization directions of the three wavelengths should be controlled using three PCs to have angles of 135°, 45°, and 135°, with respect to one principal

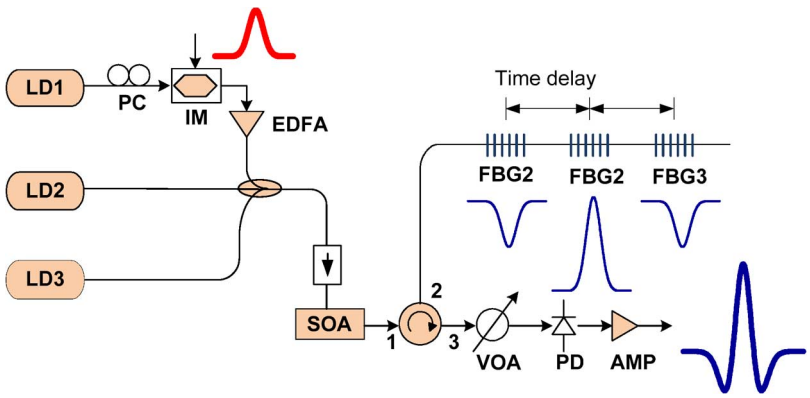

Fig. 22. UWB doublet generation using a three-tap photonic microwave delay-line filter with one negative coefficient based on XGM in an SOA.

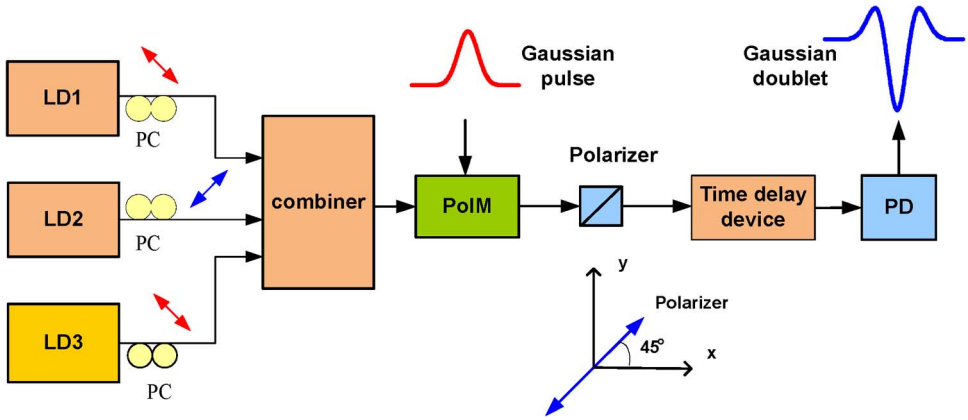

Fig. 23. UWB doublet generation using a three-tap photonic microwave delay-line filter with one negative coefficient based on XPolM in a PolM.

axis of the PolM. At the output of the PolM, a polarizer has its polarization axis adjusted to have an angle of 45° with the same principal axis of the PolM. Due to the polarization modulation, three intensity-modulated Gaussian pulses with or without polarity inversion are generated. By introducing a time-delay difference using a time-delay device (three cascaded FBGs with a reflectivity ratio of $1:2:1$), a three-tap microwave delay-line filter with coefficients of $[1\ -2\ 1]$ is realized.

Note that the negative coefficient has a magnitude that is twice that of the positive coefficients. Therefore, in designing the time-delay device, the reflection for the wavelength from LD2 should be twice that for LD1 and LD3, which can be realized by controlling the reflectivities of the three cascaded FBGs. In addition, the three FBGs should be cascaded with a physical spacing between two adjacent FBGs corresponding to the required time-delay difference.

IV. UWB Pulse Generation Based on Spectral Shaping and Frequency-to-Time Mapping

Spectral shaping and frequency-to-time mapping for ultrafast electrical pulse shaping or generation has been intensively investigated in the past few years [30]. Due to the well-known duality between paraxial diffraction in space and dispersion in time, a dispersive device, such as a dispersive fiber or a linearly chirped FBG, can serve as a real-time Fourier transformer to perform the frequency-to-time conversion [30], [31]. Dispersion-induced frequency-to-time mapping based on the space-time duality was analyzed in detail in [30]. In [32], an approach that was proposed to generate broadband arbitrary RF waveforms based on frequency-to-time mapping was implemented using free-space optics. In the approach in [32], a desirable spectrum waveform was obtained by space Fourier transform of an optical pulse using a spatial light modulator (SLM) and a Fourier lens. The temporal UWB pulses were then generated based on the frequency-to-time conversion in a dispersion medium. Optical spectral shaping and dispersive frequency-to-time mapping were also implemented to generate adaptive broadband microwave arbitrary waveforms [33] and to measure optical fiber dispersion and to evaluate an optical source spectrum [34].

A. UWB Pulse Generation Based on Optical Spectral Shaping and Frequency-to-Time Mapping

Recently, UWB pulse generation based on SLM-based spectrum shaper and frequency-to-time mapping was proposed and demonstrated [32], [35]–[38]. The major difficulty that is associated with the SLM-based approaches for UWB pulse generation is that the pulse shaping process is implemented in free space, which makes the system bulky and complicated.

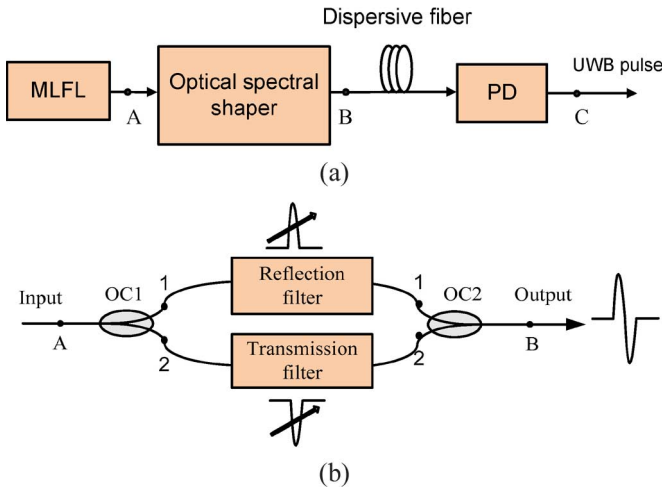

Fig. 24. (a) UWB pulse generation based on spectral shaping and frequency-to-time mapping using all-fiber components. (b) All-fiber spectrum shaper configuration.

UWB pulses can also be generated based on spectral shaping and frequency-to-time conversion using pure fiber-optic components [39]. The use of fiber-optic components instead of free-space optics has the advantage of smaller size, light weight, and the potential for integration using the photonic integrated circuit (PIC) technique.

Fig. 24(a) shows a UWB pulse generation system based on spectral shaping and frequency-to-time mapping using all-fiber components. In the system, the optical power spectrum of a femtosecond pulse from a mode-locked fiber laser (MLFL) is shaped by two optical filters to obtain a spectral shape corresponding to a UWB monocycle or a doublet. A length of SMF acting as a dispersive device is used to perform the frequency-to-time mapping and, at the same time, as a transmission medium to distribute the UWB pulse to a remote site. A UWB monocycle or doublet pulse is then obtained at the output of a high-speed PD. The UWB pulse has a shape that is a scaled version of the user-designed power spectrum. The pulsewidth is determined by the total dispersion of the SMF. As shown in Fig. 24(b), an ultrashort pulse from the MLFL source is divided into two channels by an optical coupler. The input pulse spectrum from one port is shaped by a reflection filter; the input pulse from the other port is spectrally shaped by a transmission filter. The spectra shapes of the two filters are complementary, which ensures that the time-domain pulses are polarity reversed.

The spectrum-shaped pulse is then sent to a length of dispersive fiber to perform frequency-to-time mapping. If the duration of the filtered pulse, which is denoted as Δt_0, and the chromatic dispersion χ (ps/nm) of the dispersive fiber satisfy the following relation:

$$\left|\frac{\Delta t_0^2 c}{2\pi\lambda_0^2\chi}\right| \ll 1 \tag{28}$$

where λ_0 is the center wavelength of the MLFL source, and c is the light velocity in a vacuum, then the average optical power of the output pulse is proportional to the energy spectrum of the input pulse envelope [31], i.e.,

$$|y(t)|^2 \propto |X(\omega)|^2_{\omega=(2\pi ct)/(\lambda_0^2\chi)} \tag{29}$$

where $y(t)$ is the complex envelope of output pulse, and $X(\omega)$ is the Fourier transform of the input pulse envelope. The mapping relationship of spectrum bandwidth $\Delta\lambda$ to temporal pulsewidth Δt is determined by

$$\Delta t = \chi\Delta\lambda. \tag{30}$$

Therefore, a properly determined chromatic dispersion according to (30) would yield a pulse with appropriate temporal width to ensure the UWB pulse spectrum to meet the FCC regulations. As a result, after the optical-to-electrical conversion in a high-speed PD, we can obtain a UWB monocycle or doublet pulse.

B. Implementation of All-Fiber UWB Pulse Generation Based on Spectral Shaping and Frequency-to-Time Mapping

The UWB pulse generation system, as shown in Fig. 24(a), is experimentally implemented [39]. The optical spectrum shaper can be configured to generate UWB monocycle or doublet pulse by adjusting the parameters (the spectral width and the center wavelength) of the two optical filters. The input ultrashort pulse is split into two channels by an optical coupler (OC1). To generate a UWB monocycle, the input pulse spectrum from port 1 of OC1 is shaped by a reflection filter with its center wavelength tuned at 1557.71 nm, with a 3-dB bandwidth of 0.2 nm. The input spectrum from port 2 of OC1 is shaped by a transmission filter (an FBG) with a 3-dB bandwidth of 0.25 nm and a center wavelength at 1558.2 nm. The spectrum-shaped pulses are then combined at a second optical coupler (OC2). To ensure that the positive and negative spectral peaks have an identical magnitude, the coupling ratio of OC1 can be properly selected. In the experiment, the coupling ratio is 70 : 30 since the reflection filter has higher insertion loss. The optical lengths of the two branches are carefully controlled to guarantee a temporal synchronization of optical pulses from different paths.

Fig. 25(a) shows the optical spectrum at the output of the spectrum shaper. The shaped optical spectrum exhibits a monocycle pulse shape but is superimposed on a broader Gaussian-like pedestal, which is the spectrum of the pulse from the MLFL, as shown in Fig. 25(b). The spectrally shaped optical pulse is then applied to a 10-km SMF serving as the dispersive medium to perform the frequency-to-time mapping. The total chromatic dispersion of the SMF is about 170 ps/nm. The UWB pulse that was obtained at the output of the PD is shown in Fig. 25(c). The pulse has the same shape as the optical power spectrum before mapping. The pulsewidth of the monocycle is about 185 ps, which is in good agreement with the theoretical value of 187 ps, which was calculated based on (30) using the total fiber dispersion and the monocycle pulse spectrum width. The spectrum of the generated monocycle pulse is shown in Fig. 25(d). As can be seen, the spectrum has a central frequency of 6 GHz with a 10-dB bandwidth of 9 GHz, i.e., from 1.5

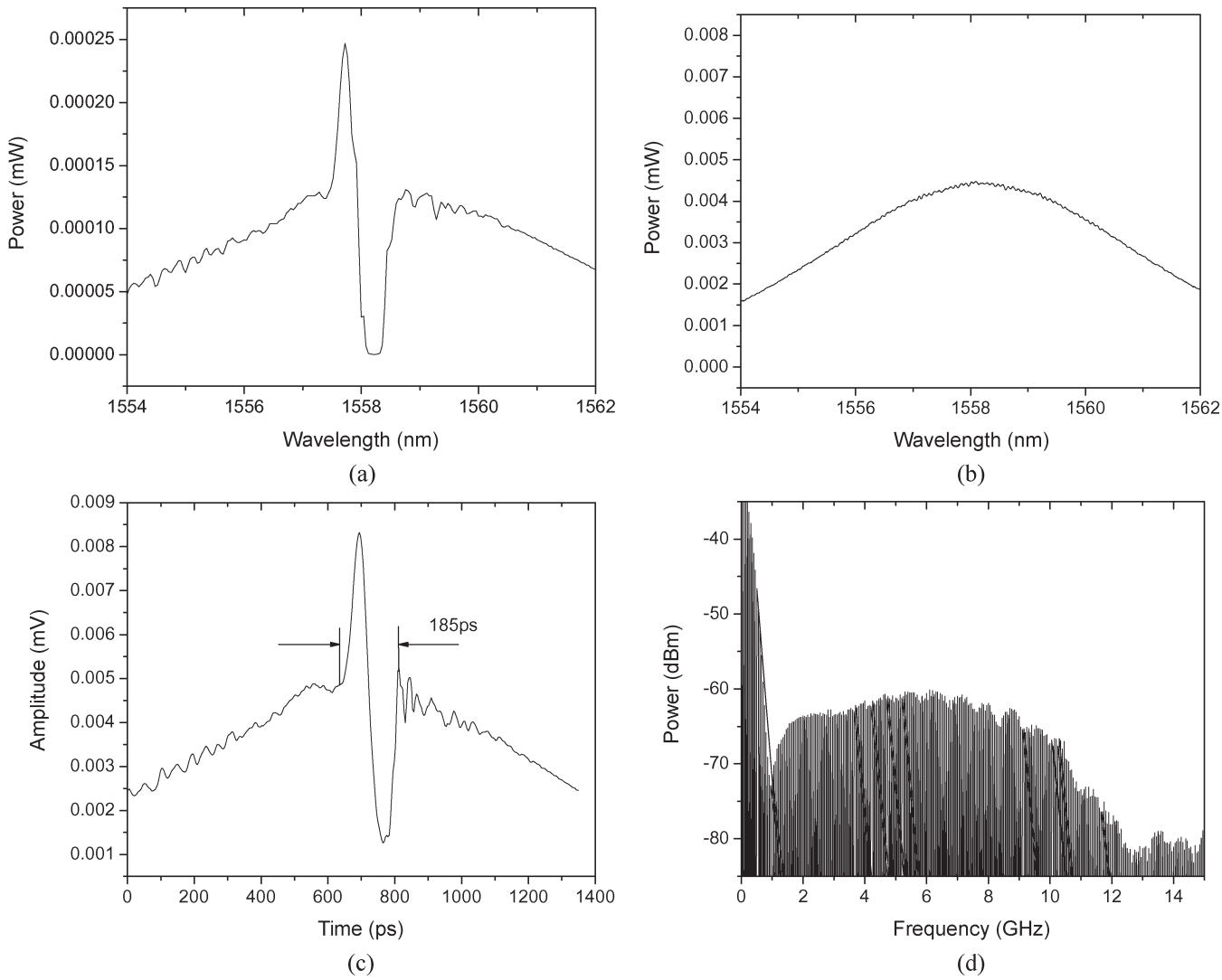

Fig. 25. All-fiber UWB monocycle pulse generation based on spectral shaping and frequency-to-time mapping. (a) Spectrum after spectral shaping. (b) Spectrum of the incident ultrashort pulse. (c) Generated UWB monocycle pulse. (d) Power spectrum of the generated monocycle pulse.

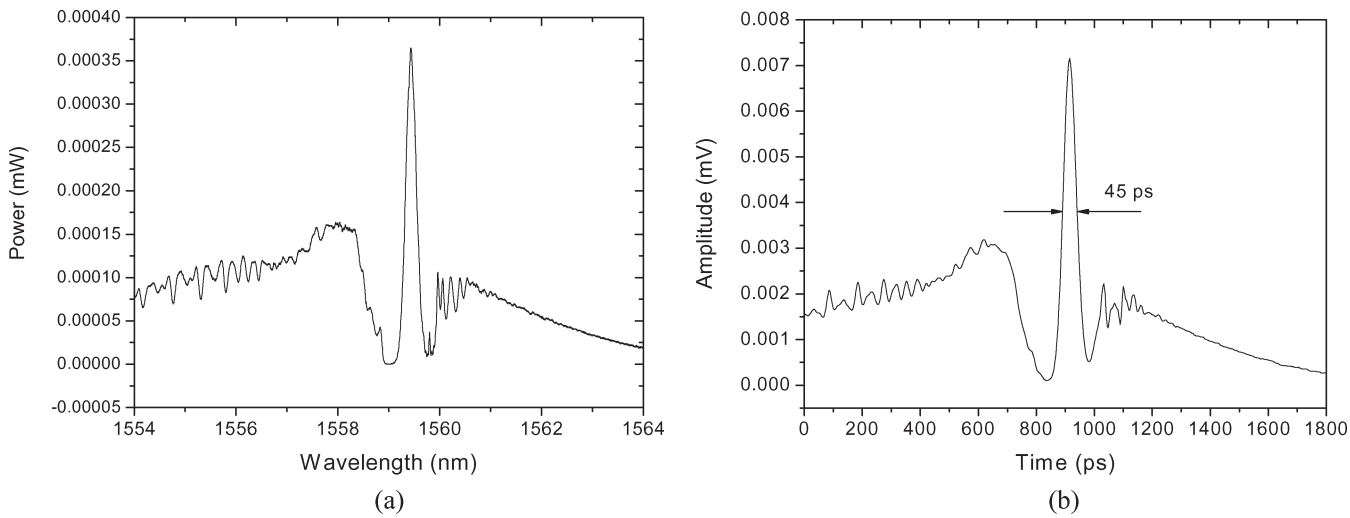

Fig. 26. UWB doublet pulse generation. (a) Spectrum after spectrum shaping. (b) Generated UWB doublet pulse.

to 10.5 GHz. The fractional bandwidth is about 150%. There is a spectral component at the baseband with a bandwidth of less than 1 GHz, as shown in Fig. 25(d), which results from the Gaussian-like pedestal. To reduce or eliminate this spectral component, we may use an MLFL with a much narrower pulse spectrum or use a dc block at the output of the PD.

To generate a UWB doublet, the spectrum shaper has to be reconfigured by using a transmission filter (an FBG) with a broader spectral width. The input pulse from port 1 of OC1 is spectrally shaped by the reflection filter, with the center wavelength set at 1559.45 nm. In the other path, the input pulse spectrum is shaped by an FBG with a broader bandwidth of 0.45 nm centered at 1559.4 nm. The spectrum-shaped optical pulses from the two arms are recombined by OC2. Fig. 26(a) shows the optical spectrum after the spectrum shaper. It has a shape corresponding to a doublet. After distribution over the 10-km SMF, a UWB doublet pulse is generated due to the dispersion-induced frequency-to-time mapping. As shown in Fig. 26(b), the generated UWB doublet pulse has an FWHM of about 45 ps, which is again superimposed on a broad and small Gaussian-like pedestal. The generated UWB doublet pulse has a 10-dB bandwidth of about 9.5 GHz, i.e., from 1.5 to 11 GHz.

V. Discussion and Conclusion

In this paper, techniques to generate UWB pulses in the optical domain have been discussed. These techniques were divided into three categories: 1) PM–IM conversion in a dispersive device, 2) microwave filtering using a photonic microwave delay-line filter having two- or three taps with one negative tap, and 3) optical spectral shaping and frequency-to-time mapping in a dispersive device. The key feature of the techniques in all the three categories is that all could be implemented using all fiber-optic components, which provide the potential for integration using integrated photonic circuits. Compared to the techniques in the second and third categories, the techniques in the first category have a simpler structure, with only a single LD required. The approach based on spectral shaping and frequency-to-time mapping in the third category has more flexibility in generating UWB pulses with arbitrary shapes. The use of an optical pulsed source may make the system more complicated and costly.

In addition to the techniques that were discussed, there are a few other techniques that were developed recently for UWB pulse generation, such as UWB generation using a frequency-shift keying modulator [40] and a nonlinearly biased Mach–Zehnder modulator [41]. The key advantage of using optics to generate UWB pulses are that the UWB pulses that were generated directly in the optical domain can be distributed over the optical fiber without the need for an extra electrical-to-optical conversion. In addition, the extremely broad bandwidth that is offered by optics enables the generation of UWB pulses with a large fractional bandwidth, which is usually difficult to realize using electronic circuits.

In a UWB-over-fiber network, a CO is connected via optical fiber to base stations or APs. Optical generation of UWB pulses is only one of the many functions in a UWB-over-fiber network. To demonstrate a practical UWB-over-fiber network, other functions should also be implemented, such as UWB pulse encoding at the CO. The pulse encoding can be implemented in the systems based on PM–IM conversion by simply switching the optical wavelength to realize PPM or PSM. A major limitation of these techniques is the limited speed of wavelength switching, which may not be suitable for a UWB communication system operating at a high data rate. In a UWB communication system, to implement the PPM or PSM, it is highly desirable that the UWB pulses can be switched at a speed that is higher than 100 MHz [2]. A technique for generating UWB pulses that is able to perform PPS and PSM at a speed of as high as 40 Gb/s has been recently demonstrated [42].

Other topics that need to be investigated for UWB-over-fiber applications include fiber dispersions and nonlinearity on the performance of the UWB-over-fiber systems. The UWB antenna design would also be a topic for further investigation.

The key challenge that limits the practical applications of UWB-over-fiber technologies for broadband wireless indoor networking is the high cost of optoelectronic components. The use of PIC technology would be a solution to reduce the cost.

References

[1] Fed. Commun. Commission, *Revision of Part 15 of the Commission's Rules Regarding Ultra-Wideband Transmission Systems*, Apr. 2002. Tech. Rep., ET-Docket 98-153, FCC02-48.

[2] M. Ghavami, L. B. Michael, and R. Kohno, *Ultra Wideband Signals and Systems in Communication Engineering*. West Sussex, U.K.: Wiley, 2004.

[3] D. Porcine, P. Research, and W. Hirt, "Ultra-wideband radio technology: Potential and challenges ahead," *IEEE Commun. Mag.*, vol. 41, no. 7, pp. 66–74, Jul. 2003.

[4] G. R. Aiello and G. D. Rogerson, "Ultra-wideband wireless systems," *IEEE Microw. Mag.*, vol. 4, no. 2, pp. 36–47, Jun. 2003.

[5] K. Siwiak and D. McKeown, *Ultra-Wideband Radio Technology*. Chichester, U.K.: Wiley, 2004.

[6] L. Q. Yang and G. B. Giannakis, "Ultra-wideband communications: An idea whose time has come," *IEEE Signal Process. Mag.*, vol. 21, no. 6, pp. 26–54, Nov. 2004.

[7] C. R. Nassar, F. Zhu, and Z. Wu, "Direct sequence spreading UWB systems: Frequency domain processing for enhanced performance and throughput," in *Proc. IEEE Int. Conf. Commun.*, May 2003, vol. 3, pp. 2180–2186.

[8] J. Balakrishnan, A. Batra, and A. Dabak, "A multi-band OFDM system for UWB communication," in *Proc. IEEE Conf. Ultra Wideband Syst. Technol.*, Nov. 16–19, 2003, pp. 354–358.

[9] X. Wu, Z. Tian, T. N. Davidson, and G. B. Giannakis, "Optimum waveform design for UWB radios," *IEEE Trans. Signal Process.*, vol. 54, no. 6, pp. 2009–2021, Jun. 2006.

[10] H. Ishida and K. Araki, "Design and analysis of UWB bandpass filter with ring filter," in *IEEE MTT-S Int. Tech. Dig.*, Jun. 2004, vol. 3, pp. 1307–1310.

[11] L. Zhu, S. Sun, and W. Menzel, "Ultra-wideband (UWB) bandpass filters using multiple-mode resonator," *IEEE Microw. Wireless Compon. Lett.*, vol. 15, no. 11, pp. 796–798, Nov. 2005.

[12] W. P. Lin and J. Y. Chen, "Implementation of a new ultrawide-band impulse system," *IEEE Photon. Technol. Lett.*, vol. 17, no. 11, pp. 2418–2420, Nov. 2005.

[13] F. Zeng and J. P. Yao, "All-optical bandpass microwave filter based on an electro-optic phase modulator," *Opt. Express*, vol. 12, no. 16, pp. 3814–3819, Aug. 2004.

[14] F. Zeng and J. P. Yao, "Investigation of phase modulator based all-optical bandpass filter," *J. Lightw. Technol.*, vol. 23, no. 4, pp. 1721–1728, Apr. 2005.

[15] J. Wang, F. Zeng, and J. P. Yao, "All-optical microwave bandpass filters implemented in a radio-over-fiber link," *IEEE Photon. Technol. Lett.*, vol. 17, no. 8, pp. 1737–1739, Aug. 2005.

[16] F. Zeng and J. P. Yao, "All-optical microwave mixing and bandpass filtering in a radio-over-fiber link," *IEEE Photon. Technol. Lett.*, vol. 17, no. 4, pp. 899–901, Apr. 2005.
[17] J. P. Yao, G. Maury, Y. L. Guennec, and B. Cabon, "All-optical subcarrier frequency conversion using an electrooptic phase modulator," *IEEE Photon. Technol. Lett.*, vol. 17, no. 11, pp. 2427–2429, Nov. 2005.
[18] Y. Le Guennec, G. Maury, J. P. Yao, and B. Cabon, "New optical microwave up-conversion solution in radio-over-fiber networks for 60 GHz wireless applications," *J. Lightw. Technol.*, vol. 24, no. 3, pp. 1277–1282, Mar. 2006.
[19] J. Wang, F. Zeng, and J. P. Yao, "All-optical microwave bandpass filters with negative coefficients based on PM-IM conversion," *IEEE Photon. Technol. Lett.*, vol. 17, no. 10, pp. 2176–2178, Oct. 2005.
[20] F. Zeng, J. Wang, and J. P. Yao, "All-optical microwave bandpass filter with negative coefficients based on an electro-optic phase modulator and linearly chirped fiber Bragg gratings," *Opt. Lett.*, vol. 30, no. 17, pp. 2203–2205, Sep. 2005.
[21] F. Zeng and J. P. Yao, "An approach to ultra-wideband pulse generation and distribution over optical fiber," *IEEE Photon. Technol. Lett.*, vol. 18, no. 7, pp. 823–825, Mar. 2006.
[22] F. Zeng and J. P. Yao, "Ultrawideband signal generation using a high-speed electrooptic phase modulator and an FBG-based frequency discriminator," *IEEE Photon. Technol. Lett.*, vol. 18, no. 19, pp. 2062–2064, Oct. 2006.
[23] X. Chen and S. Kiaei, "Monocycle shapes for ultra wideband system," in *Proc. IEEE Int. Symp. Circuits Syst.*, 2002, vol. 1, pp. 26–29.
[24] F. Zeng, Q. Wang, and J. P. Yao, "All-optical UWB impulse generation based on cross phase modulation and frequency discrimination," *Electron. Lett.*, vol. 43, no. 2, pp. 119–121, Jan. 2007.
[25] A. J. Seeds, "Microwave photonics," *IEEE Trans. Microw. Theory Tech.*, vol. 50, no. 3, pp. 877–887, Mar. 2002.
[26] R. A. Minasian, "Photonic signal processing of microwave signals," *IEEE Trans. Microw. Theory Tech.*, vol. 54, no. 2, pp. 832–846, Feb. 2006.
[27] J. Capmany, B. Ortega, and D. Pastor, "A tutorial on microwave photonic filters," *J. Lightw. Technol.*, vol. 24, no. 1, pp. 201–229, Jan. 2006.
[28] Q. Wang, F. Zeng, S. Blais, and J. P. Yao, "Optical UWB monocycle pulse generation based on cross-gain modulation in a semiconductor optical amplifier," *Opt. Lett.*, vol. 31, no. 21, pp. 3083–3085, Nov. 2006.
[29] J. P. Yao and Q. Wang, "Photonic microwave bandpass filter with negative coefficients using a polarization modulator," *IEEE Photon. Technol. Lett.*, vol. 19, no. 9, pp. 644–646, May 2007.
[30] A. M. Weiner, "Femtosecond pulse shaping using spatial light modulators," *Rev. Sci. Instrum.*, vol. 71, no. 15, pp. 1929–1960, May 2000.
[31] M. Muriel, J. Azaña, and A. Carballar, "Real-time Fourier transformer based on fiber gratings," *Opt. Lett.*, vol. 24, no. 1, pp. 1–3, Jan. 1999.
[32] I. Lin, J. D. McKinney, and A. M. Weiner, "Photonic synthesis of broadband microwave arbitrary waveforms applicable to ultra-wideband communication," *IEEE Microw. Wireless Compon. Lett.*, vol. 15, no. 4, pp. 226–228, Apr. 2005.
[33] J. Chou, Y. Han, and B. Jalali, "Adaptive RF-photonic arbitrary waveform generator," *IEEE Photon. Technol. Lett.*, vol. 15, no. 4, pp. 581–583, Apr. 2003.
[34] Y. C. Tong, L. Y. Chan, and H. K. Tsang, "Fiber dispersion or pulse spectrum measurement using a sampling oscilloscope," *Electron. Lett.*, vol. 33, no. 11, pp. 983–985, May 1997.
[35] B. Jalali, J. Chou, and H. Yan, "Optically sculpt UWB waveforms," *Microw. RF*, vol. 43, no. 8, pp. 54–62, Aug. 2004.
[36] J. D. McKinney, I. S. Lin, and A. M. Weiner, "Shaping the power spectrum of ultra-wideband radio-frequency signals," *IEEE Trans. Microw. Theory Tech.*, vol. 54, no. 12, pp. 4247–4255, Dec. 2006.
[37] S. Xiao and A. M. Weiner, "Programmable photonic microwave filters with arbitrary ultra-wideband phase response," *IEEE Trans. Microw. Theory Tech.*, vol. 54, no. 11, pp. 4002–4008, Nov. 2006.
[38] J. D. McKinney and A. M. Weiner, "Compensation of the effects of antenna dispersion on UWB waveforms via optical pulse-shaping techniques," *IEEE Trans. Microw. Theory Tech.*, vol. 54, no. 4, pp. 1681–1686, Jun. 2006.
[39] C. Wang, F. Zeng, and J. P. Yao, "All-fiber ultra wideband pulse generation based on spectral shaping and dispersion-induced frequency-to-time conversion," *IEEE Photon. Technol. Lett.*, vol. 19, no. 3, pp. 137–139, Feb. 2007.
[40] T. Kawanishi, T. Sakamoto, and M. Izutsu, "Ultra-wide-band signal generation using high-speed optical frequency-shift-keying technique," in *IEEE Int. Top. Meeting MWP—Tech. Dig.*, 2004, pp. 48–51.
[41] Q. Wang and J. P. Yao, "UWB doublet generation using a nonlinearly-biased electro-optic intensity modulator," *Electron. Lett.*, vol. 42, no. 22, pp. 1304–1305, Oct. 2006.
[42] Q. Wang and J. P. Yao, "An electrically switchable optical ultra-wideband pulse generator," *J. Lightw. Technol*, vol. 25, no. 11, pp. 3626–3633, Nov. 2007.

Jianping Yao (M'99–SM'01) received the Ph.D. degree in electrical engineering from the Université de Toulon, Toulon, France, in 1997.

From 1999 to 2001, he held a faculty position with the School of Electrical and Electronic Engineering, Nanyang Technological University, Singapore. In 2001, he joined the School of Information Technology and Engineering, University of Ottawa, Ottawa, ON, Canada, where he is currently a Professor, the Director of the Microwave Photonics Research Laboratory, and the Director of the Ottawa-Carleton Institute for Electrical and Computer Engineering. He is a Guest Professor with Shantou University, Shantou, China, and Sichuan University, Chengdu, China, and was an Invited Professor with the Institut National Polytechnique de Grenoble, Grenoble, France, in 2005. His research has focused on microwave photonics, which includes all-optical microwave signal processing; photonic generation of microwaves, millimeter waves, and terahertz; radio over fiber; UWB over fiber; fiber Bragg gratings for microwave photonics applications; and optically controlled phased array antennas. His research interests also include fiber lasers, fiber-optic sensors, and biophotonics. He has published more than 160 papers in refereed journal and conference proceedings.

Dr. Yao is a member of the International Society for Optical Engineers and the Optical Society of America and is a Senior Member of the IEEE Lasers and Electro-Optics Society and of the IEEE Microwave Theory and Techniques Society. He is a Registered Professional Engineer in the province of Ontario.

Fei Zeng (S'04–M'07) received the B.Eng. degree in optoelectronic engineering from Huazhong University of Science and Technology, Wuhan, China, in 1993 and the M.A.Sc. and Ph.D. degrees in electrical engineering from the School of Information Technology and Engineering, University of Ottawa, Ottawa, ON, Canada, in 2003 and 2006, respectively.

From 1993 to 2001, he was with NEC Fiber Optical Communications Ltd., Wuhan, working on synchronous digital hierarchy and dense wavelength-division multiplexing system verification. He is currently with the Research Laboratory of Electronics, Massachusetts Institute of Technology, Cambridge. His research interests include microwave photonics and photonic nanostructures for biosensing, nanomanipulation, and biospectroscopy.

Dr. Zeng is a Student Member of the Optical Society of America.

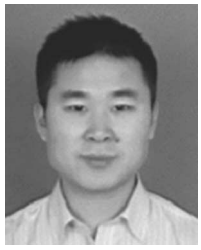

Qing Wang received the B.Eng. and Ph.D. degrees in electronic engineering from Tsinghua University, Beijing, China, in 2000 and 2006, respectively.

In March 2006, he joined the Microwave Photonics Research Laboratory, School of Information Technology and Engineering, University of Ottawa, Ottawa, ON, Canada, as a Postdoctoral Researcher. His research interests include fiber amplifiers and lasers, fiber Bragg gratings, nonlinearities in fiber and semiconductor-based optical devices, and microwave photonic signal generation and processing.